

# 激光通信天线一体化的摆镜面形优化

李小明<sup>1,2\*</sup>, 王隆铭<sup>2</sup>, 李响<sup>1,2</sup>, 张立中<sup>1,2</sup>, 张家齐<sup>1</sup>

<sup>1</sup>长春理工大学空间光电技术国家地方联合工程研究中心, 吉林 长春 130022;

<sup>2</sup>长春理工大学机电工程学院, 吉林 长春 130022

**摘要** 一对多激光通信天线受结构和尺寸的限制, 反射镜与安装平面只能单独研磨。虽然可根据面形测试结果对安装平面进行反复研磨, 以保证摆镜安装后的面形精度, 但该方法难度大、周期长、成功率低。为了减小加工难度, 在保证正常研磨精度( $5\ \mu\text{m}$ )的同时降低安装面平面度造成的安装应力和温度变形等外力影响, 保证摆镜安装后的面形精度。研究了摆镜在力学作用下的面形精度变化和面形稳定性, 优化设计了隔离结构, 有效提高了摆镜的面形稳定性。测试结果表明, 在测试波长为  $\lambda$  时, 安装应力和温度升(降)载荷作用下摆镜面形精度的峰谷值由  $0.546\lambda$  提升到  $0.161\lambda$ , 均方根值由  $0.099\lambda$  提升到  $0.019\lambda$ , 完全符合设计要求。

**关键词** 激光通信; 摆镜; 优化设计; 面形精度

中图分类号 TH89

文献标志码 A

doi: 10.3788/CJL202148.0106006

## 1 引言

激光通信具有速率高、抗干扰能力强、体积小、功耗低等优势, 可突破现有微波通信速率的瓶颈, 能有效解决高速大容量信息实时传输的问题<sup>[1-2]</sup>。随着激光通信技术的不断发展, 以激光通信为骨干链路的全光网络受到了广泛的研究, 用激光通信构建一体化高速信息网络也是我国未来的发展方向, 国内多家单位已经开展了相关的规划与研究工作。全光网络中要求各节点具备信息的实时交互功能, 因此, 需要具有组网功能的一对多光通信终端, 以实现全光网络的组网通信。传统激光通信只能实现一对一的点对点通信, 严重制约了激光通信技术的组网应用<sup>[3-5]</sup>, 因此, 研究一对多激光通信技术具有重要意义。

一对多激光通信室内原理验证系统中, 天线可以用多面具有独立光轴对准功能的摆镜协同工作, 在大范围内实现一对多激光通信。为了提高摆镜的反射效率, 保证多镜动态拼接时的能量利用率, 对摆镜组件的结构尺寸和镜面到转动中心的距离提出了更高的要求。本文设计了一体化紧凑型摆镜, 但实验和测试结果表明, 摆镜对安装面平面度的要求较高。受结构和工艺的限制, 其安装面加工难度较大, 因此, 还需对一体化摆镜进行优化设计, 降低安装面平面度造成的影响, 保证摆镜安装后的面形精度。

## 2 紧凑型摆镜

一对多激光通信光学天线设计为多摆镜拼接结构, 每块摆镜由一个伺服执行机构驱动, 以实现对目标的稳定跟踪<sup>[6-7]</sup>。来自不同通信目标的信号光以不同入射角照射到多摆镜拼接光学天线上时, 工作范围与入射光角度匹配的摆镜对目标进行跟踪, 以保证通信光能进入系统中<sup>[8]</sup>。天线模型如图 1(a)所示, 每个摆镜都可以独立完成跟踪捕获, 相邻两个摆镜可以进行拼接, 从而提高激光收发效率并完成目标的交替跟踪、扩大跟踪范围。二维摆镜组件如图 1(b)所示, 由方位轴系、俯仰轴系和摆镜组成, 摆镜通过安装板与俯仰轴系连接并在方位和俯仰轴系的带动下进行二维转动。根据室内实验使用环境要求, 在测试波长为  $\lambda$ 、摆镜面形的温度为  $(20 \pm 5)\ ^\circ\text{C}$  时, 波面的峰谷值(PV)优于  $0.167\lambda$ , 均方根值(RMS)优于  $0.020\lambda$ 。

摆镜一般用背部柔性支撑结构隔离热载荷或安装引起的外力, 以保证摆镜的面形精度。本系统中的支撑机构设计在摆镜背部, 不易与镜体一起加工, 且会增大俯仰回转轴心与镜面的距离, 不利于轻小型化。因此, 系统的摆镜采用一体化设计, 将与镜体一体化的安装板直接安装在俯仰轴系的侧面。摆镜和俯仰轴安装座均选用比刚度高、加工性好、体积分

收稿日期: 2020-06-30; 修回日期: 2020-07-30; 录用日期: 2020-08-31

基金项目: 国家自然科学基金重大研究计划(91338116)

\* E-mail: lxmkkid@163.com

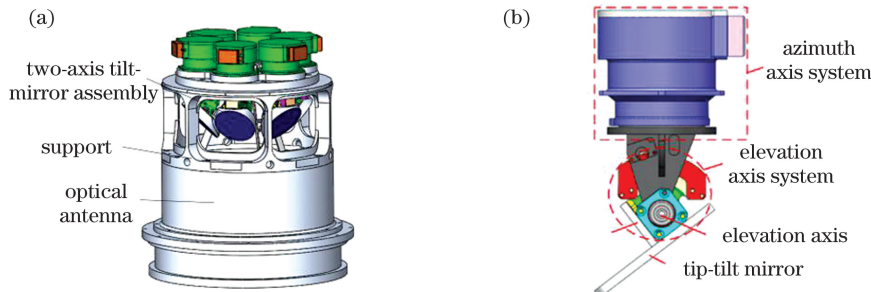


图 1 一对多激光通信天线系统。(a) 天线;(b) 二维摆镜组件

Fig. 1 One-to-many laser communication antenna system. (a) Antenna; (b) two-axis tilt-mirror assembly

数高的新型材料 SiC/Al,按光学要求将摆镜设计成长轴为 100 mm、短轴为 80 mm 的椭圆形镜面,预留尺寸为 30 mm×30 mm×54 mm 的轴系安装空间,摆镜的结构如图 2(a)所示。优化设计后摆镜的镜面厚度为 20 mm,加强筋的宽度为 10 mm,质量为 220 g。研究表明,在重力作用下面形误差的 PV 为

$0.018\lambda$ ,RMS 为  $0.0038\lambda$ ,这表明摆镜的刚度较好。摆镜与安装座通过三个螺钉连接,安装座在螺钉连接处设计有凸台,以减小摆镜与安装座的接触面积、保证安装面的研磨精度,从而减小接触面的平面度误差,摆镜组件如图 2(b)所示。图 2(c)和图 2(d)分别为摆镜和安装座的实物图。

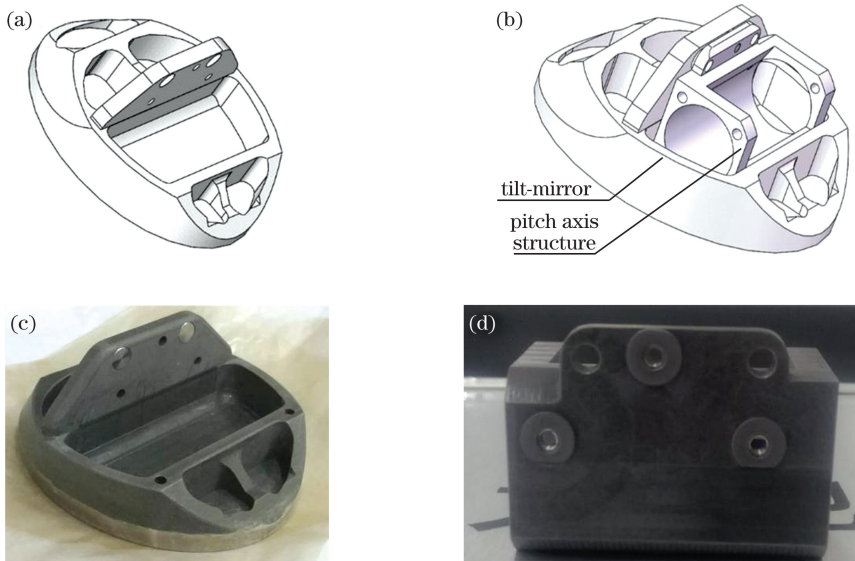


图 2 一体化的摆镜组件。(a) 摆镜模型;(b) 组件装配图;(c) 摆镜;(d) 安装座

Fig. 2 Integrated tilt-mirror assembly. (a) Model of tilt-mirror; (b) assembly drawing of components; (c) tilt-mirror; (d) mounting seat

摆镜的材料采用体积分数较高的 SiC/Al,但 SiC/Al 的稳定性不好,容易造成镜面精度退化。因此,摆镜在完成加工镀膜后还需对其面形进行多次间隔检测,即将反射镜放置一段时间后再测试摆镜的面形精度和面形稳定度。测试结果表明,摆镜放置 7 d 后的面形 PV 为  $0.091\lambda$ ,RMS 为  $0.014\lambda$ ,放置 12 d 后的面形 PV 为  $0.093\lambda$ ,RMS 为  $0.015\lambda$ ,这表明摆镜自身的面形稳定度较好。

传统摆镜一般将支撑机构与轴系间的安装面配合研磨,连接后再对摆镜的反射面进行精抛加工,然

后安装在系统中,以保证面形精度<sup>[9-10]</sup>。为了最大限度地减小回转轴系与镜面的距离,将轴系安装座深入到镜体内部,安装俯仰轴系时需要拆分,因此,安装面只能独立进行研磨然后安装。测试结果表明,在研磨误差为  $5 \mu\text{m}$ (受研磨工艺和检测精度的限制)时,摆镜安装后的面形精度无法满足设计要求,必须根据摆镜安装后的面形检测结果对安装面进行多次修磨。但其迭代修磨次数多、难度大、成功率较低,且系统有 3 面独立的摆镜,导致加工周期长、难度大。因此,优化摆镜时还需额外考虑研磨误

差等因素对面形精度的影响,从而减小对安装面面形精度的要求。

### 3 安装面平面度对面形精度的影响

如图3(a)所示,摆镜通过安装座上的三个安装点连接,忽略安装座凸台的面积,将摆镜简化为A、B、C三点。设研磨后安装面的平面度最大误差为 $p_{\max}$ ,即相比理想平面ABC,某一点处有垂直

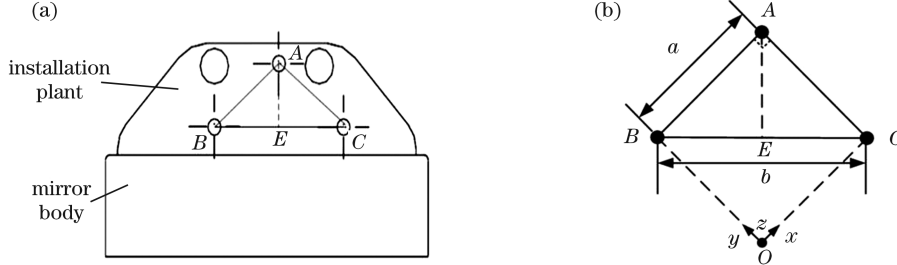


图3 摆镜的安装结构。(a)安装点的布局;(b)安装点的简化模型

Fig. 3 Installation structure of tilt-mirror. (a) Layout of installation points; (b) simplified model of installation points

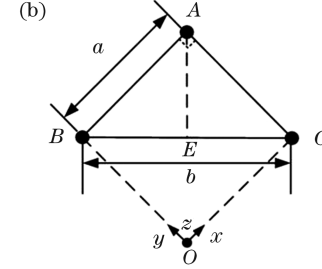
设平面度误差造成安装点A在垂直平面方向发生了强制位移 $p_{\max}$ ,将经过A点并垂直于BC的安装板截面等效为一长度为l的悬臂板条梁,则A点的反作用力F和强制位移 $p_{\max}$ 的关系为<sup>[11]</sup>

$$E_l I p_{\max} = \frac{F}{3} l^3, \quad (1)$$

$$F = \frac{3E_l I p_{\max}}{l^3}, \quad (2)$$

式中, $E_l = E/(1-\mu^2)$ 为板条梁的相当弹性模量, $I=t^3/12$ 为板条梁的断面惯性矩, $E=200$  GPa为SiC/Al的弹性模量, $\mu=0.3$ 为材料的泊松比, $t=10$  mm为安装板的厚度, $p_{\max}=5$   $\mu\text{m}$ 。经计算得到 $F=0.0175$  N。由于安装板属于刚性板,变形较小,

于平面距离为 $p_{\max}$ 的强制位移。在螺钉作用下,其余两点保持不动且不可旋转,安装板会产生一定内力和变形并沿安装板向镜体传递。为简化计算,将安装板简化为一矩形平板,A、B、C分别为矩形板的三个顶点,O为矩形的第四个顶点,且 $AB=AC=a$ , $AB \perp AC$ ,点E为BC的中点,建立坐标系O-xyz,设 $AE=20$  mm, $BC=50$  mm,如图3(b)所示。



因此假设:1)板变形前垂直于中面的法线,变形后仍为直线;2)忽略板在厚度方向上的正应力;3)忽略板中面的变形。在该假设条件下边BO和CO为固定边,根据弹性理论,自由支撑在刚性周界上的板边界条件为<sup>[12]</sup>

$$\begin{cases} \omega_x = 0, \left(\frac{\partial^2 \omega}{\partial x^2}\right)_{x=0} = 0 \\ \omega_y = 0, \left(\frac{\partial^2 \omega}{\partial y^2}\right)_{y=0} = 0 \end{cases}, \quad (3)$$

式中, $\omega$ 为整体挠度, $\omega_x$ 为x轴的挠度, $\omega_y$ 为y轴的挠度, $\left(\frac{\partial^2 \omega}{\partial x^2}\right)_{x=0}$ 为x的二阶导数, $\left(\frac{\partial^2 \omega}{\partial y^2}\right)_{y=0}$ 为y的二阶导数,边AB和AC为自由边, $AB=AC=a$ 的边界条件为

$$\begin{cases} \left(\frac{\partial^2 \omega}{\partial x^2} + \mu \frac{\partial^2 \omega}{\partial y^2}\right)_{x=a} = 0, \left[\frac{\partial^3 \omega}{\partial x^3} + (2-\mu) \frac{\partial^3 \omega}{\partial x \partial y^2}\right]_{x=a} = 0 \\ \left(\frac{\partial^2 \omega}{\partial y^2} + \mu \frac{\partial^2 \omega}{\partial x^2}\right)_{y=a} = 0, \left[\frac{\partial^3 \omega}{\partial y^3} + (2-\mu) \frac{\partial^3 \omega}{\partial x^2 \partial y}\right]_{y=a} = 0 \end{cases}. \quad (4)$$

设安装面的挠度方程为 $\omega(x, y) = mxy$ ,其中, $m$ 为一常数。当挠度方程满足上述边界条件时,有

$$-F = F_{RAB} + F_{RAC} = (M_{yx})_A + (M_{xy})_A = 2(M_{xy})_A = -2E_l I (1-\mu) \left(\frac{\partial^2 \omega}{\partial x \partial y}\right)_{x=y=a}, \quad (5)$$

式中, $F_{RAB}$ 为沿AB向的横向切力, $F_{RAC}$ 为沿AC向的横向切力, $(M_{xy})_A$ 为y绕x轴方向上的内力,

$(M_{xy})_A$ 为x绕y轴方向上的内力,由于力臂相等,即 $AB=AC=a$ ,可得到

$$m = \frac{F}{2E_l I (1-\mu)}, \quad (6)$$

$$\omega(x, y) = \frac{F}{2E_l I (1-\mu)} xy. \quad (7)$$

由于BC中点E处的挠度为 $2.13 \times 10^{-4}$  mm,

根据双端支撑简支梁的挠度方程,可得到

$$E_I I \omega = -F_E l_E^3 / 24, \quad (8)$$

式中,  $l_E$  为边  $AE$  的长度,  $E$  点处的等效载荷  $F_E = 7.49 \times 10^{-4}$  N。

通过(2)式~(8)式可计算  $A$ 、 $C$  点固定,  $B$  (或  $C$ ) 点发生  $5 \mu\text{m}$  的强制位移(沉陷)时,  $B$  (或  $C$ ) 点的反作用力  $F_B = 0.0063$  N,  $E$  点的相对挠度为  $7.6 \times 10^{-5}$  mm 时的等效载荷为  $2.67 \times 10^{-4}$  N。这表明摆镜安装面的平面度误差会使安装板变形并产生内力,且  $A$  点产生沉陷时对镜面的影响大于  $B$  点和  $C$  点。

仿真分析了摆镜不同安装点产生  $5 \mu\text{m}$  沉陷和  $5^\circ\text{C}$  温变载荷对面形精度的影响,结果如图 4(a)~图 4(d) 所示。可以发现,安装面平面度对摆镜面形精度的影响较大,如图 4(a) 中  $A$  点沉陷时,摆镜面形的 PV 为  $186$  nm, RMS 为  $45.2$  nm; 如图 4(b) 中  $B$  点沉陷时,摆镜面形的 PV 为  $126$  nm, RMS 为  $23$  nm; 如图 4(c) 中  $C$  点沉陷时,摆镜面形的 PV 为  $127$  nm, RMS 为  $24$  nm, 无法满足设计要求。为进一步验证分析结果,对图 4(d) 所示的摆镜(安装面研磨精度为  $5 \mu\text{m}$ , 三座标检测安装面的平面度为  $4.8 \mu\text{m}$ ),用干涉仪检测不同安装点螺钉紧定时的镜面面形变化,紧定时采用力矩扳手校紧,保证接触

面充分贴合,校紧力矩为  $5 \text{ N} \cdot \text{m}$ , 测试结果如图 4(e)~图 4(i) 所示。从图 4(e) 可发现,摆镜自由状态下面形的 PV 为  $0.095\lambda$  ( $60$  nm), RMS 为  $0.015\lambda$  ( $9.5$  nm); 从图 4(f) 可知,3 个安装螺钉全部锁紧后,摆镜面形的 PV 为  $0.546\lambda$  ( $345$  nm), RMS 为  $0.099\lambda$  ( $63$  nm); 从图 4(g) 可发现,单独放松  $A$  螺钉后面形的 PV 为  $0.24\lambda$  ( $151$  nm), RMS 为  $0.046\lambda$  ( $29$  nm), 与 3 个螺钉全部紧定时的面形数据相比,不平整导致摆镜面形 PV 的变化量为  $194$  nm, RMS 变化量为  $53.5$  nm; 从图 4(h) 可知,单独放松  $B$  螺钉后面形的 PV 为  $0.377\lambda$  ( $234$  nm), RMS 为  $0.053\lambda$  ( $33.5$  nm), 不平整导致摆镜面形的 PV 变化量为  $121$  nm, RMS 变化量为  $24$  nm; 从图 4(i) 可以发现,单独放松  $C$  螺钉后面形的 PV 为  $0.335\lambda$  ( $208$  nm), RMS 为  $0.062\lambda$  ( $39.5$  nm), 不平整导致摆镜面形 PV 的变化量为  $137$  nm, RMS 变化量为  $30$  nm。具体实验结果如表 1 所示,可以发现,实验结果与理论分析一致,安装点  $A$  的沉陷对面形精度的影响最大,此时面形精度无法满足优于  $12$  nm ( $0.020\lambda$ ) 的设计要求;且安装面研磨误差在螺钉紧定后会导致摆镜面变形,造成安装后摆镜面形质量下降。

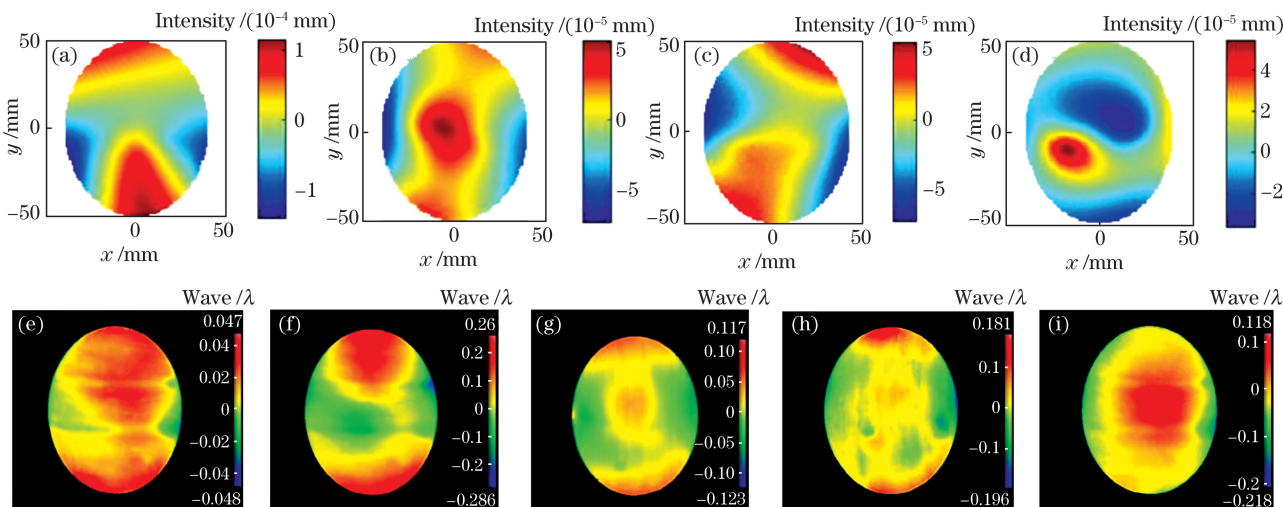


图 4 不同安装点的面形变化。(a)  $A$  点; (b)  $B$  点; (c)  $C$  点; (d)  $5^\circ\text{C}$  温升(降)下的面形变化; (e) 自由状态下的面形变化; (f) 螺钉锁紧时的面形变化; (g)  $A$  点松动的面形变化; (h)  $B$  点松动的面形变化; (i)  $C$  点松动的面形变化

Fig. 4 Surface shape changes of different mounting points. (a) Point  $A$ ; (b) point  $B$ ; (c) point  $C$ ; (d) surface shape change under  $5^\circ\text{C}$  temperature rise(drop); (e) surface shape change in free state; (f) surface shape change when the screw is tightened; (g) surface shape change when the point  $A$  is loose; (h) surface shape change imitates when the point  $B$  is loose; (i) surface shape change when the point  $C$  is loose

表 1 安装点对面形精度的影响

Table 1 Influence of the installation point on the surface accuracy

unit: nm

Operation mode	Analysis result			Test result		
	A	B	C	A loose	B loose	C loose
PV	186.0	126.0	127.0	194.0	121.0	137.0
RMS	45.2	23.0	24.0	53.50	24.0	30.0

## 4 摆镜面形优化

为了在保证摆镜结构紧凑的同时减小外力对面形精度的影响,提高摆镜面形的稳定性,必须隔离变形向镜体的传递,因此在安装板上设计如图 5 所示的隔离槽,以减小安装面的柔度,有效隔离安装力的传递,更便于安装板与摆镜的一体化加工。

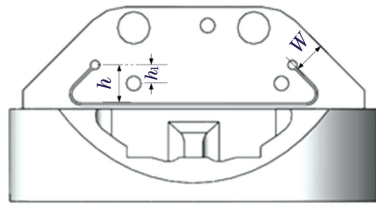


图 5 隔离槽的示意图

Fig. 5 Schematic diagram of isolation tank

隔离槽的主要参数有侧臂宽度  $W$  以及槽顶高度  $h$ 。当 A 点产生沉陷时,根据挠度公式得到高度为  $h$  点的挠度  $\omega_h$ 、弯矩  $M_h$  和作用力  $F$  的关系为

$$E_I \omega_h = \frac{F}{6} h^3 - \frac{F}{2} h_1 h^2, \quad (9)$$

$$\frac{d^2 \omega_h}{dh^2} = \frac{M_h}{E_I I}. \quad (10)$$

由安装点沉陷引起高度为  $h$  处安装面的弯矩为

$$M_h = Fh - Fh_1, \quad (11)$$

式中,  $h_1$  为隔离槽定点与安装点的距离。弯距通过侧臂在与摆镜镜体连接面上产生的应力为

$$\sigma = \frac{M_h}{W_z} = \frac{6(Fh - Fl)}{tW^2}, \quad (12)$$

式中,  $W_z = tW^2/6$  为侧臂的抗弯截面系数。

由(12)式可知,增加隔离槽的高度和侧臂宽度有利于减小安装点沉陷引起的镜体集中应力,增加侧臂宽度有利于提高摆镜的动态刚度,但增加隔离槽的高度会减小动态刚度,优化时为使摆镜的刚度大于 300 Hz,需保证侧臂宽度并优化隔离槽高度。受支撑点位置和加工工艺的影响,侧臂与支撑点 C 的距离为 5 mm,侧臂宽度为 7 mm,隔离槽宽为

0.5 mm。槽两端留有直径  $\varphi$  为 2 mm 的工艺孔,方便穿丝和减小应力集中,隔离槽与摆镜镜体顶面的距离为 1 mm,可保证切割过程中不会损伤镜体结构。在上述参数的基础上对隔离槽高度  $h$  进行优化,目标函数为在 A 点沉陷 5  $\mu\text{m}$  时,安装面面形精度的 PV 小于 0.033 $\lambda$ , RMS 小于 0.010 $\lambda$ ,以保证原始面形的 PV 小于 0.125 $\lambda$ , RMS 小于 0.017 $\lambda$ ,安装面研磨精度为 5  $\mu\text{m}$  的条件下,摆镜安装后的面形满足 PV 小于 0.167 $\lambda$ , RMS 小于 0.020 $\lambda$  的设计要求,且摆镜的一阶模态大于 150 Hz。

优化后的隔离槽高度为 9.5 mm,图 6(a)为高面形稳定摆镜,图 6(b)为二维摆镜组件的实物图,图 6(c)和图 6(d)为优化后摆镜 A 点沉陷和 5 °C 温升(降)载荷下的面形变化结果。有限元分析结果表明,在 A 点施加 5  $\mu\text{m}$  的强制位移时,反射面 PV 的最大误差小于 0.027 $\lambda$ , RMS 小于 0.010 $\lambda$ , 5 °C 温升(降)时的面形 PV 小于 0.031 $\lambda$ , RMS 小于 0.008 $\lambda$ ,摆镜在三个安装点固定时的一阶谐振频率为

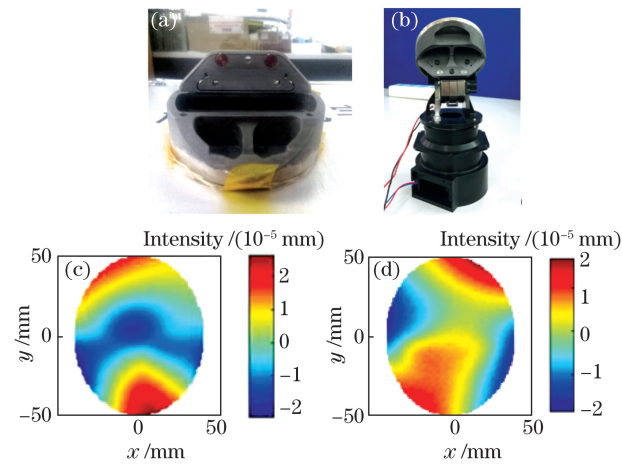


图 6 优化后摆镜的实物和面形变化。(a) 摆镜;(b) 二维摆镜组件;(c) A 点沉陷时的面形变化;(d) 5 °C 温升(降)时的面形变化

Fig. 6 Physical and surface change of the tilt-mirror after optimization. (a) Tilt-mirror; (b) two-axis tilt-mirror assembly; (c) surface change when point A sinks; (d) surface change when temperature rises (drops) at 5 °C

520 Hz。可以发现,优化后摆镜的镜面变形明显减小,摆镜的面形稳定性得到了很大提高,对外力影响的抑制能力得到了加强,可以保证摆镜安装后达到设计指标要求。

## 5 实验与测试

采用干涉仪检测优化后摆镜的面形精度,图 7(a)为检测装置,将摆镜安装在调架上,安装面的研磨精度  $4.8 \mu\text{m}$ 。首先在不紧定三个安装螺钉(摆镜处于自由状态)下,检测无安装应力下的初始面,结果如图 7(b)所示;然后将三个安装螺钉全部紧定,检测结果如图 7(c)所示;最后在( $20 \pm 5$ ) °C 时检测摆镜的面形,结果如图 7(d)所示,表 2 为摆镜面形的检测结果及对比。

从表 2 可以发现,优化的摆镜安装后的面形精度得到了控制,面形变化率由优化前的 77.5% (PV) 和 60% (RMS) 下降到 13.8% (PV) 和 6.5% (RMS)。这表明优化后的摆镜高效隔离了安装对面形精度的影响,进一步提升了面形的稳定性。优化后的一体化摆镜在安装面平面度误差为  $4.8 \mu\text{m}$  和 5 °C 温升(降)条件下的面形 PV 为  $0.161\lambda$ , RMS

表 2 摆镜面形的测试结果  
Table 2 Test result of tilt-mirror surface shape

Test object	Before optimization		After optimization	
	PV	RMS	PV	RMS
Free state/ $\lambda$	0.095	0.015	0.115	0.016
Screw lock/ $\lambda$	0.546	0.099	0.133	0.017
Rate of change/%	77.500	60.000	13.800	6.500
5 °C temperature change/ $\lambda$	-	-	0.161	0.019

图 8(a)为一对多激光通信天线实物图,系统在激光端机的配合下成功开展了一点同时对三点、通信速率 2.5 Gbit/s 的室内多点激光通信演示实验。

为  $0.019\lambda$ ,满足 PV 小于  $0.167\lambda$ , RMS 小于  $0.020\lambda$  的设计要求。

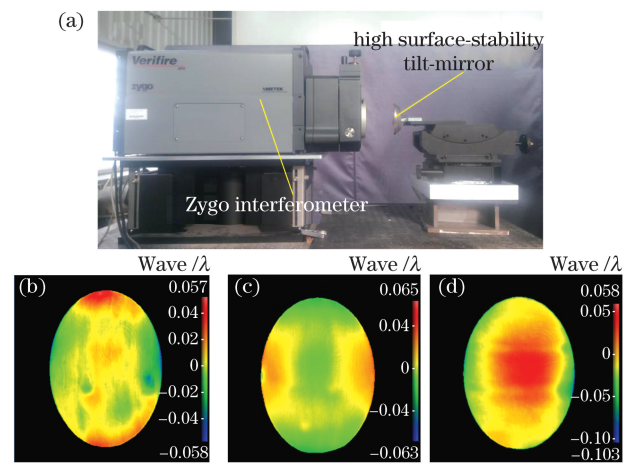


图 7 面形的检测结果。(a)面形测试装置;(b)自由状态下的一面形;(c)螺钉紧定后面形;(d)5 °C 温升(降)时的一面形

Fig. 7 Test results of surface shape. (a) Test device of surface shape; (b) surface shape in free state; (c) surface shape when screw is tightened; (d) surface shape at 5 °C temperature rise (drop)

演示现场如图 8(b)所示,一对多天线接收到激光光斑如图 8(b)中的左下角图像所示。

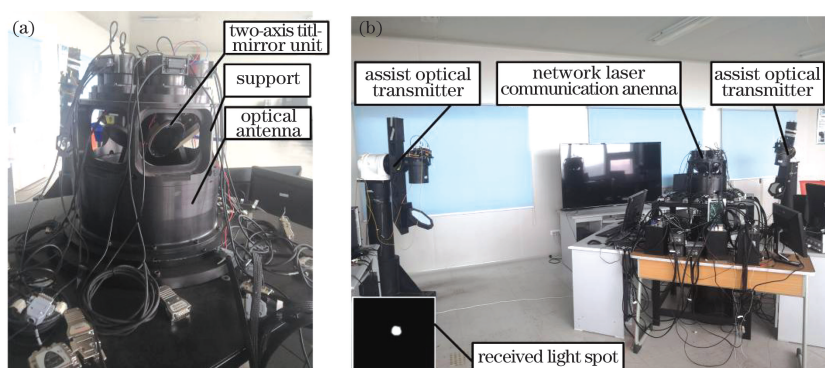


图 8 一对多激光通信的演示系统。(a)一对多激光通信天线;(b)演示现场

Fig. 8 Demonstration system of one-to-many laser communication. (a) One-to-many laser communication antenna; (b) demonstration site

精跟踪相机的帧频可以达到每秒 300 frame, 每个像素的分辨率为  $8 \mu\text{rad}$ , 因此, 采用相机自带的图像处理软件, 对截取的静态(指向但不跟踪)和动态(动态跟踪)精跟踪相机中的光斑进行识别处理, 提取光斑在  $x$  和  $y$  方向上的像元信息。光斑及软件界面如图 9 所示, 检测结果如表 3 所示。对比不同状态、不同时刻的光斑尺寸变化, 可以发现, 光斑的圆整度较好, 在动态条件下光斑的圆整度略有下降, 但影响较小。光斑测试结果也表明光斑的圆整度较好, 这表明摆镜的面形精度较高, 未对光束产生明显的破坏。

表 3 光斑尺寸的测试结果  
Table 3 Test results of spot size

Number	Status	Number of pixels in $x$ direction	Number of pixels in $y$ direction
1	static state	13.4	16.0
2	static state	12.8	16.4
3	dynamic tracking	14.6	18.8
4	dynamic tracking	14.8	17.4
5	dynamic tracking	14.0	17.6

## 6 结 论

以一对多激光通信系统中的紧凑型摆镜为研究对象, 通过理论分析和有限元仿真对摆镜面形的稳定性进行了优化。首先分析了安装点参数对摆镜镜面的影响, 优化了一体化摆镜的安装点位置, 设计了一体化摆镜安装点的位置参数; 然后针对摆镜加工与安装方式的特殊性, 分析了安装面研磨误差对面形的影响; 随后设计了隔离结构抑制平面度对面形精度的影响, 保证了一体化摆镜安装后的面形稳定性; 最后进行了面形精度测试, 结果表明, 优化后摆镜面形的 PV 小于  $0.161\lambda$ , RMS 小于  $0.019\lambda$ , 这表明该一体化摆镜在安装面平面度和温度载荷影响下完全符合设计要求。

## 参 考 文 献

- [1] Jiang H. Space laser communication technology and system [M]. Beijing: National Defence Industry Press, 2010: 9-22.  
姜会林. 空间激光通信技术与系统 [M]. 北京: 国防工业出版社, 2010: 9-22.
- [2] Song Y S, Chang S, Tong S F, et al. Feature analysis of aeronautical laser communication system and airborne laser communication experiment [J]. Chinese Journal of Lasers, 2016, 43(12): 1206004.  
宋延嵩, 常帅, 佟首峰, 等. 航空激光通信系统的特
- [3] Zhang T, Fu Q, Li Y H, et al. Design of confocal reflection optical antenna of multi-platform network laser communication [J]. Acta Optica Sinica, 2015, 35(10): 1022006.  
张涛, 付强, 李亚红, 等. 多平台激光通信组网共焦点反射式光学天线设计 [J]. 光学学报, 2015, 35(10): 1022006.
- [4] Zheng Y, Fu Y G, Hu Y, et al. Research on four-mirror dynamic alignment based on space laser communication link networks [J]. Chinese Journal of Lasers, 2014, 41(1): 0105001.  
郑阳, 付跃刚, 胡源, 等. 基于空间激光通信组网四反射镜动态对准研究 [J]. 中国激光, 2014, 41(1): 0105001.
- [5] Jiang H L, Hu Y, Song Y S, et al. Research on space laser communication network [J]. Spacecraft Recovery & Remote Sensing, 2011, 32(5): 52-59.  
姜会林, 胡源, 宋延嵩, 等. 空间激光通信组网光端机技术研究 [J]. 航天返回与遥感, 2011, 32(5): 52-59.
- [6] Jiang H L, Jiang L, Song Y S, et al. Research of optical and APT technology in one-point to multi-point simultaneous space laser communication system [J]. Chinese Journal of Lasers, 2015, 42 (4): 0405008.  
姜会林, 江伦, 宋延嵩, 等. 一点对多点同时空间激光通信光学跟瞄技术研究 [J]. 中国激光, 2015, 42(4): 0405008.



图 9 精跟踪光斑及分析结果

Fig. 9 Precision tracking spot and analysis results

- [7] Li X, Zhang L Z, Li X M, et al. Design of compact tip-tilt mirror assembly in multi-node laser communication antennas [J]. Acta Optica Sinica, 2017, 37(9): 0906003.  
李响, 张立中, 李小明, 等. 多节点激光通信天线紧凑形摆镜组件设计[J]. 光学学报, 2017, 37(9): 0906003.
- [8] Meng L X, Zhao D X, Zhang L Z, et al. Research on acquisition and tracking system for space laser communication networking [J]. Journal of Changchun University of Science and Technology (Natural Science Edition), 2014, 37(6): 70-76.  
孟立新, 赵丁选, 张立中, 等. 激光通信组网用捕跟踪机构设计[J]. 长春理工大学学报(自然科学版), 2014, 37(6): 70-76.
- [9] Qi G, Wang S X, Li J L. Design of high volume fraction SiC/Al composite mirror in space remote sensor [J]. Chinese Optics, 2015, 8(1): 99-106.  
齐光, 王书新, 李景林. 空间遥感器高体积分数SiC/Al复合材料反射镜组件设计[J]. 中国光学, 2015, 8(1): 99-106.
- [10] Jia S Q, Huang W, Pang W B. Influence of adhesive thickness on surface deformation of mirror supported by three-point mount [J]. Optics and Precision Engineering, 2015, 23(7): 2005-2012.  
贾树强, 黄玮, 庞武斌. 胶层厚度对三点支撑反射镜面形的影响[J]. 光学精密工程, 2015, 23(7): 2005-2012.
- [11] Liu H W. Mechanics of Material-II [M]. 4th ed. Beijing: Higher Education Press, 2004: 176-185.  
刘鸿文. 材料力学-II [M]. 4 版. 北京: 高等教育出版社, 2004: 176-185.
- [12] Xu Z L. Elasticity: volume 1 [M]. 5th ed. Beijing: Higher Education Press, 2016: 6-12.  
徐芝纶. 弹性力学-上册 [M]. 5 版. 北京: 高等教育出版社, 2016: 6-12.

## Optimization of Integrated Tilt-Mirror for Laser Communication Antenna

Li Xiaoming<sup>1,2\*</sup>, Wang Longming<sup>2</sup>, Li Xiang<sup>1,2</sup>, Zhang Lizhong<sup>1,2</sup>, Zhang Jiaqi<sup>1</sup>

<sup>1</sup>National and Local Joint Engineering Research Center of Space Optoelectronics Technology, Changchun University of Science and Technology, Changchun, Jilin 130022, China;

<sup>2</sup>College of Mechanical and Electrical Engineering, Changchun University of Science and Technology, Changchun, Jilin 130022, China

### Abstract

**Objective** In the one-to-many laser communication indoor principle verification system, the antenna adopts multi-faceted tilt-mirror with independent optical axis alignment function to realize one point and multi-point laser communication in a broad range. To reduce the size and working envelope of the tilt-mirror in the laser communication ground test system to meet the limitation for size, a compact and integrated tilt-mirror with SiC/Al is proposed in this paper. The tilt-mirror can be connected to the turntable's pitch axis seat to reduce the reflecting surface's eccentric distance and the whole machine's outer envelope size. The tilt-mirror and supporting structure's mounting surface can only be separately grinded and then installed since the structure restrict the system. The test shows that when the grinding accuracy is  $5 \mu\text{m}$ , the tilt-mirror profile accuracy cannot meet the design requirements. The mounting surface must also be repaired by grinding several times according to the surface inspection results after the tilt-mirror is installed. However, the system has three independent tilt-mirrors, which makes the repair grinding cycle long and complicated. Thus, the tilt-mirror must be optimized to consider the impact of grinding errors on the surface quality and reduce the requirements for the surface quality of the mounting surface. This study focuses on the tracking tilt-mirror structure in the networked laser communication ground demonstration prototype, which causes the reflector and mounting base unable to use the traditional bonding process and can only be installed with screws, resulting in serious degradation of the reflector surface during the screw connection process. Theoretical and simulation analyses are conducted to verify the reasons and laws of the problem based on the original structure's test results. It then optimized the design to improve the mirror surface's stability, ensuring that the design requirements are met.

**Methods** First, the initial design mirror's surface shape changes under different mounting points are tested. The theoretical calculations are conducted based on the experimental and test results of the original reflector structure. The analysis proves that the unevenness of the structure's installation points affects the mirror surface's accuracy. The law is consistent with the test results. Next, through finite element analysis, the influence of each installation

point of the original structure is simulated, and compared with the test result, the reason and law of the problem are verified. It is obtained that the conventional grinding and other mechanical methods cannot meet the requirements. Thus, the tilt-mirror needs to be optimized and improved. The flexible structure is then used to isolate the stress transmission, and the tilt-mirror is optimized based on the original design. The flexible structure with isolation trenches is used to solve the problem of surface degradation. Therefore, isolation grooves are designed on the mounting plate to reduce the mounting surface's flexibility and effectively isolate the installation force's transmission. The analysis showed that the surface deformation of the high-quality surface tilt-mirror reduced significantly. Also, the surface stability of the tilt-mirror has significantly been improved. The ability to suppress the external forces influence is greatly enhanced, ensuring that the tilt-mirror meets the design index requirements after installation. Finally, it verified the mirror surface's accuracy through static surface testing and verified its practical application effect through dynamic spot detection.

**Results and Discussion** The surface quality test shows that the tilt-mirror surface shape's peak-valley value is better than  $\lambda/6$ , and the root-mean-square value is better than the  $\lambda/52$  (**Fig. 7** and **Table 2**). It shows that the integrated tilt-mirror with high surface stability guarantees its surface stability under the influence of installation flatness and temperature load and fully meets the design requirements. In multi-laser communication antennas using the high-surface stability integrated tilt-mirror mirrors and indoor demonstration experiments, the camera's image processing software is used to identify the light spot in the fine tracking camera when capturing static (pointing but no tracking) and dynamic (dynamic tracking), and extract the light spot's pixel information in the  $x$ - and  $y$ -axes directions (**Fig. 9**). Comparing the changes in spot size in different states and at different times, it can be seen that the spot roundness is better, and the spot roundness is slightly reduced under dynamic conditions, but the effect is small (**Table 3**).

**Conclusion** Aiming at the problems that the structure limits the compact tilt-mirror in the networked laser communication system, the grinding accuracy of the mounting surface affects the surface accuracy of the reflecting surface, and the surface accuracy after installation is remarkably reduced and cannot meet the design requirements, the stability of the tilt-mirror surface is optimized through theoretical analysis and finite element simulation. The mechanical characteristics of the integrated tilt-mirror installation are analyzed and investigated. The influence of the installation point parameters on the surface of the tilt-mirror is analyzed. The installation point position of the integrated tilt-mirror is optimized, and the parameters of the integrated tilt-mirror are designed. Because of the particularity of the tilt-mirror processing and installation methods, the flatness' influence law and strength are analyzed. The isolation structure is designed to suppress the flatness' influence, ensuring the integrated tilt-mirror's surface stability after installation. The surface accuracy test results show that the tilt-mirror fully meets the design requirements after installation.

**Key words** laser communications; tilt-mirror; optimization design; surface quality

**OCIS codes** 060.2605; 120.4880; 130.1750